Preparation and application of self-healing hydrogel dressing based on Schiff base bonding

Lei Wang,[1] Rui Zhu,[1] ChengXiang Wang,[1] PengYi Zhao,[1] JiaXin Liu,[1] HuiPing Tang,[1] Hua-Jun Shawn Fan,[1,]*
[1] College of Chemical Engineering, Sichuan University of Science and Engineering, Zigong City, Sichuan Province, P. R. China, 64300.
* Correspondence: Dr. Hua-Jun Shawn Fan

Abstract: *Chronic wound healing disorders are closely related to the dynamic imbalance of its pathological microenvironment, and traditional dressings are difficult to meet the needs of wound microenvironment regulation due to single function, lack of dynamic responsiveness and uncontrollable drug release. Based on this, this chapter proposes to construct a novel composite hydrogel Curcumin/GQDs@OHA-CMCS. Its design strategies include: using oxidized hyaluronic acid (OHA) and carboxymethyl chitosan (CMCS) as matrix, and constructing self-healing hydrogel through dynamic Schiff base crosslinking to simulate the extracellular matrix microenvironment; The surface functionalization of GQDs was used to modify the load Cur to realize the coordination of mechanical performance improvement and efficient drug delivery, and the fluorescence characteristics of GQDs were used to monitor the drug release behavior in real time. This chapter will focus on the preparation process, physicochemical properties characterization, drug release and in vitro biological activity of hydrogels, providing theoretical basis for the development of intelligent hydrogels with high drug loading, controlled release and real-time monitoring functions.*
Keywords: *Self-healing hydrogels; GQDs; Curcumin; Wound dressings; Hyaluronic acid*

I.   Introduction

As the largest organ system in the human body and the primary barrier to external aggression, skin tissue plays a key role in maintaining homeostasis of the internal environment. The long-term exposure of the skin to the complex external environment makes it the organ most likely to be traumatized [1]. Clinical data show that the annual demand for trauma treatment in China has exceeded 100 million cases, of which chronic non-healing wounds account for 30%, which is closely related to the accelerated ageing of the population and the increasing prevalence of metabolic diseases (e.g. diabetes mellitus) [2]. Poor wound healing not only significantly prolongs the treatment period, but can also lead to serious infections and even life-threatening conditions. Current clinical treatment strategies include surgical debridement, skin grafting and anti-infective drug interventions [3][4]. Wound dressings play an irreplaceable role in tissue repair through the mechanisms of physical barrier formation, wound exudate management and infection prevention and control. However, with the deepening of the concept of precision medicine, the development of smart dressings with active repair function has become an important research direction in the field of biomaterials. Current wound dressings can be broadly classified into two types: traditional dressings and novel dressings. Traditional dressings (gauze, bandages, cotton balls, etc.) have cost advantages but have inherent defects such as adhesion to the wound, poor permeability and limited protective efficacy [5]. The continuous development of science and technology has led to the emergence of new wound dressings, including film dressings, foam dressings, hydrogel dressings and bioactive dressings [6]. The new wound dressings should not only have the basic physical protection function of traditional wound dressings, but also have innovative performance enhancements and incorporate a variety of effects while strengthening the basic functions. The concept of self-healing is derived from the self-healing ability in biology, and most organisms have the ability to heal and regenerate themselves after external damage. Inspired by the self-healing phenomena of organisms (e.g. DNA repair, epidermal regeneration, etc.) [7] self-healing hydrogels achieve structural and functional reconstruction of materials after damage by mimicking the damage response mechanism of living systems. Schiff bases can be reversibly reacted under mild conditions, allowing the hydrogel to rapidly recover its structure and function after damage [8]. In addition, the pH-responsive properties of Schiff base hydrogels allow them to undergo network structure dissociation in the mildly acidic environment of bacterial infection, further releasing the active materials loaded into the hydrogel. Therefore, Schiff base hydrogels have excellent drug delivery capabilities and can be loaded with antibiotics [9], metal nanoparticles [10], self-assembled nanoparticles [11][12] and other drug. Chen et al [13] combined antibiotics with amino groups and protocatechuic acid with aldehyde groups via Schiff base bonding and verified that the amino groups on the surface of the drug correlated with its loading. This chemically bound loading of the drug in a hydrogel can significantly improve the

release behavior of the drug. Hydrogels have been the focus of wound healing dressing research in the last decade, and self-healing polysaccharide hydrogel systems based on dynamic imine bonding have shown unique advantages in the field of wound repair [14]. Hydrogels prepared based on the Schiff base reaction have several advantages such as injectability, self-healing, in situ forming and good biocompatibility, and have been widely used in the fields of drug carriers and cell culture [15-19]. For example, chitosan-oxidized konjac-glucan composite hydrogel was adapted to irregular wounds by injectable molding with good adhesion, self-healing ability and biocompatibility, which significantly shortened the wound healing cycle [20]. In terms of drug delivery, the ethylene glycol chitosan/polyethylene glycol self-healing hydrogel could achieve slow release of paclitaxel with a longer release time than the traditional Pluronic F127 hydrogel system. In addition, the dopamine-modified sodium alginate-polyacrylamide system combines high tensile strength and super ductility through the synergistic action of multiple dynamic bonds (hydrogen bonding, Schiff base bonding), and a large number of catechol groups on the OSA-DA chain can provide the hydrogel with unique cell affinity and tissue adhesion [21]. Such materials have been extended to hemostasis, anti-tumor and cartilage repair [22][23], marking the evolution of self-healing hydrogels towards functional integration.

In response to the dynamic changes in the microenvironment of chronic wounds and the need for stepwise treatment, this study proposes a three-dimensional construction strategy of 'dynamic network support, intelligent carrier response and active molecule synergy'. Hyaluronic acid (HA) has abundant hydroxyl and carboxyl groups on its main chain, which can be oxidized to form aldehyde groups or modified by acylation to form acyl groups, providing active sites for the Schiff base reaction. However, hyaluronic acid suffers from poor stability, short half-life and susceptibility to degradation, which limits its clinical application [24][25]. By modifying hyaluronic acid prior to the reaction, the above shortcomings can be overcome, allowing hyaluronic acid to have a wider range of biomedical applications. Etherification of a large number of hydroxyl and amino groups within chitosan yields water-soluble carboxymethyl chitosan (CMCS), which has good antimicrobial and anticancer activities, good biocompatibility and superior biodegradability properties. As a new generation derivative of carbon-based nanomaterials, Graphene Quantum Dots (GQDs) are ideal candidates for drug delivery systems due to their unique photoluminescence (PL) properties, excellent water solubility and biocompatibility. Compared with traditional carbon materials, the surface of GQDs is rich in carboxyl, hydroxyl and other active functional groups, which can be functionalized through covalent bonding, π-π stacking and hydrogen bonding, which provides a molecular basis for its use as an efficient drug delivery carrier. Curcumin, a diketone compound with good biocompatibility and biodegradability, is potentially useful in the prevention and treatment of a wide range of diseases due to its diverse effects such as anti-inflammatory [26], antimicrobial [27], antioxidant [28] and anticancer [29]. However, the poor water solubility and low oral bioavailability of curcumin have limited its use in clinical practice. In this study, a novel composite hydrogel, Curcumin/GQDs@OHA-CMCS, was proposed to be constructed. Its design strategies include: using oxidized hyaluronic acid (OHA) and carboxymethyl chitosan (CMCS) as matrix, and constructing self-healing hydrogel through dynamic Schiff base cross-linking to simulate the extracellular matrix microenvironment; The surface functionalization of GQDs was used to modify the load Cur to realize the coordination of mechanical performance improvement and efficient drug delivery, and the fluorescence characteristics of GQDs were used to monitor the drug release behavior in real time. This chapter will focus on the preparation process, physicochemical properties characterization, drug release and in vitro biological activity of hydrogels, providing theoretical basis for the development of intelligent hydrogels with high drug loading, controlled release and real-time monitoring functions.

II.   Methods

2.1 Preparation of GQDs-NH$_2$

1.993 g of pyrene (Pyrene, purity $\geq$98%) was weighed into a 500 mL three-necked flask, and 165 mL of concentrated nitric acid (HNO$_3$, 70%) was slowly added dropwise through a constant pressure funnel at room temperature. After the dropwise addition, the reaction system was heated to 80 °C and stirred at reflux for 12 h. After the reaction, the reaction solution was cooled down to room temperature, transferred to a beaker and diluted with water to neutralize the excess nitric acid until the pH of the solution was close to neutral. Subsequently, the precipitate was collected by vacuum filtration and washed with deionized water three times to remove the residual acid. The yellow solid product was finally placed in a vacuum drying oven and dried at room temperature for 12 h to obtain 1,3,6-trinitropyrene powder (1,3,6-trinitropyrene). Next, 0.3119 g of 1,3,6-trinitropyrene was weighed, added with 55 mL of deionized water and 5 mL of concentrated ammonia (NH$_3$-H$_2$O, 30%) and ultrasonicated for 4 h in an ice-water bath, to obtain a homogeneous orange-yellow suspension. The suspension was transferred to a 100 mL PTFE-lined autoclave, sealed and placed in an oven and heated at 200 °C for 10 h. After the reaction, the reactor was cooled down to room temperature, the product solution was collected and centrifuged (12000 r/min, 20 min) to remove large impurities, and the supernatant was then filtered through a 0.22 μm microporous membrane. After filtration, the filtrate was concentrated to about 1/3 of the original volume under reduced pressure in a rotary evaporator, and the concentrate was dialyzed in deionized water using a dialysis bag with a molecular

weight cut-off of 14,000 (Mw = 14 kDa) for 2 d to purify the product, during which the dialysate was changed at least three times a day. The purified GQDs-NH$_2$ solution was placed in a freeze dryer and dried under vacuum at -60°C for 48 h to obtain a final dark brown GQDs-NH$_2$ solid powder.

2.2 Preparation of Curcumin/GQDs

The preparation of graphene quantum dots (GQDs-NH$_2$)-loaded curcumin (Cur) was achieved by a simple mixing method: an ethanol solution of Cur (1.5 mL, 1.25 mg/mL) was mixed with a dispersion of GQDs (1.5 mL, 1 mg/mL, with solvent being a 50:50 (v/v) mixing system of ethanol and water), and the mixture was stirred for 24 h at room temperature and protected from light to promote Cur's physical Adsorption. The final product was washed repeatedly with anhydrous ethanol and then centrifuged and filtered (12000 r/min, 20 min), and then secondly filtered with 0.22 μm microporous membrane to remove unbound free Cur molecules, and then finally dried under vacuum at -60°C for 48 h to obtain Cur-loaded GQD nanoparticles (Curcumin/GQDs). Drug loading was achieved by π-π stacking with hydrophobic interactions, and dark environment operation effectively avoided the photosensitive degradation of Cur.

2.3 Preparation of Curcumin/GQDs@OHA-CMC hydrogels

OHA-CMCS hydrogels were prepared by mixing 10% (w/v) OHA solution and 5% (w/v) CMCS solution in a 1:2 (v/v) ratio at room temperature. Subsequently, Curcumin/GQDs@OHA-CMCS hydrogels, referred to as CG@OC hydrogels, were prepared by homogeneously doping 20 mg of Curcumin/GQDs into CMCS-OHA hydrogels.

III. Results and Discussion
3.1 Study on morphology, structure and chemical composition of Curcumin/GQDs

As shown in the **Figure 1**, the morphology characterization of amino functionalized graphene quantum dots (GQDs-NH2) by atomic force microscopy (AFM) shows that the prepared nanoparticles have a uniform point size distribution, and the statistical average longitudinal height is about 4.3 nm, reflecting good monodispersion characteristics. Raman spectral analysis showed that the prepared GQDs-NH2 showed significant characteristic vibration peaks at 1331 cm^{-1} and 1592 cm^{-1}, which were attributed to the D and G peaks of carbon atom crystals, respectively. X-ray diffraction (XRD) results show that GQDs-NH$_2$ has an obvious diffraction peak at 27.2°, which corresponds to the characteristic peak of the graphite (002) surface, indicating that the material has a good crystal structure and a high degree of graphitization. In addition, the infrared spectroscopic analysis of the prepared GQDs-NH$_2$ further revealed the chemical characteristics of its surface functional groups. The strong absorption peak at 3429 cm^{-1} is attributed to the stretching vibration of N-H/O-H groups on the material surface, where the significant contribution of N-H indicates the successful introduction of amino groups. The absorption peaks at 2925 cm^{-1} and 2858 cm^{-1} correspond to the stretching vibration of C-H bonds, respectively, which may come from alkyl or methyl groups on the surface or substrate of the material. The characteristic peak at 1617 cm^{-1} corresponds to the stretching vibration of the C=C bond, reflecting the conjugated structure of the carbon skeleton in the graphene quantum dots. The absorption near 1381 cm^{-1} may be related to the stretching vibration of the C-N bond, while the peak at 1162 cm^{-1} can be attributed to the vibration pattern of the C-O-C or C-N functional group. The above infrared characteristics indicate that GQDs-NH$_2$ successfully achieves amino functionalization, and its surface has both hydrophobic carbon skeleton and hydrophilic functional group, which provides the structural basis for the fluorescence response and drug loading in the subsequent hydrogel system.
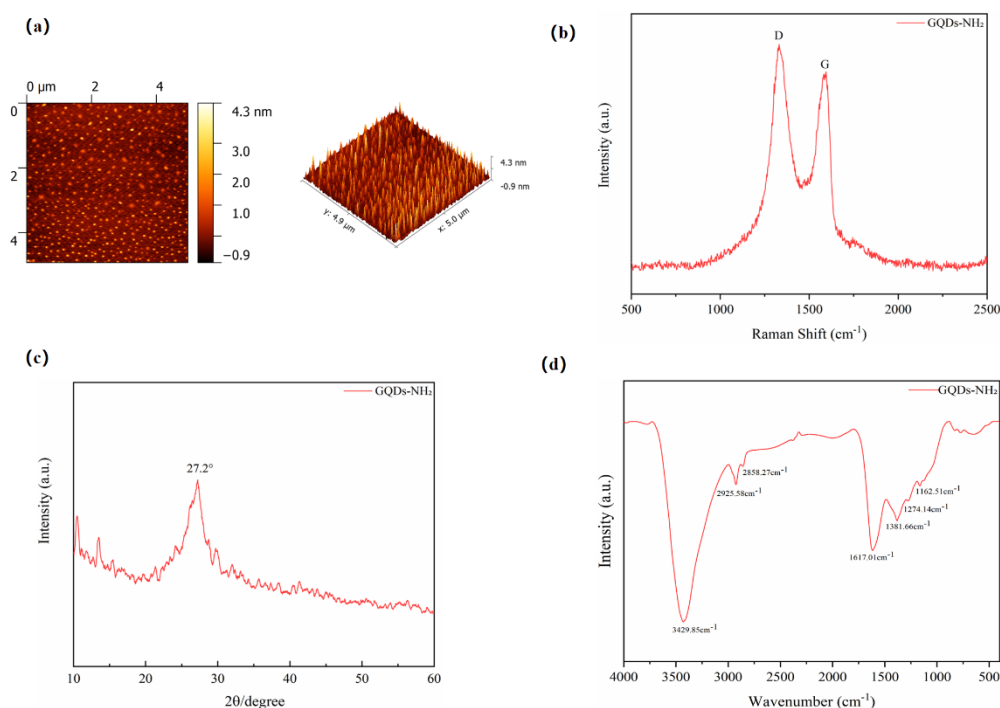
Figure 1 (a)AFM topography, (b)Raman spectra, (c)XRD spectra and (d)IR spectra of GQDs-NH$_2$

The optical properties of the prepared GQDs-NH$_2$ were characterized by UV-VIS absorption spectra and photoluminescence spectra. As shown in the **Figure 2**, the UV-visible absorption spectra show two characteristic peaks around 257 nm and 316 nm, corresponding to the π-π transition of the C=C bond in the aromatic carbon framework and the n-π transition of the surface carbonyl group (C=O), respectively, indicating that the quantum dots have a hybrid structure of both sp² conjugative domains and oxygen-containing functional groups. Further analysis of its fluorescence properties shows that the maximum excitation wavelength of GQDs-NH$_2$ is 340 nm, and the corresponding maximum emission wavelength is 429 nm, indicating that the material has a stable fluorescence emission ability in the blue region. This clear excitation-emission wavelength mapping provides the basis for its application as a fluorescence probe, especially when GQDs-NH$_2$ is introduced into a hydrogel system, whose fluorescence properties can dynamically respond to changes in the local microenvironment (such as pH, ion concentration, or intermolecular interactions caused by drug release) during drug release. In addition, the visible region emission of GQDs-NH$_2$ (429 nm) overlaps less with the ultraviolet absorption bands of most hydrogel substrates and drug molecules, and its wide excitation spectrum (maximum excitation 340 nm) further reduces background interference, providing a high signal-to-noise ratio optical signal for real-time and in-situ monitoring. Therefore, it shows potential application value in visual tracking of drug controlled release system.
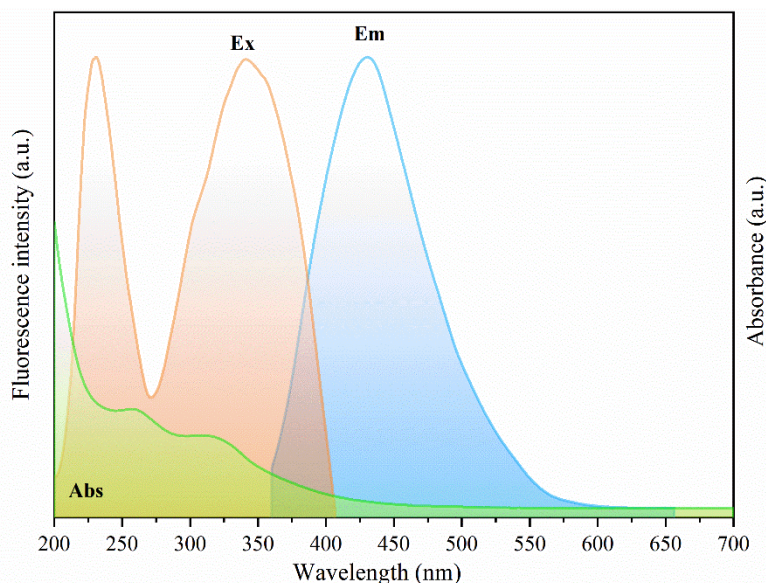
Figure 2 Uv absorption and PL spectra of GQDs-NH$_2$

3.2 Curcumin/GQDs@OHA-CMCS Morphology observation and analysis of infrared spectrum results

As shown in **Figure 3**(a), it can be seen that Curcumin/GQDs@OHA-CMCS hydrogel has a continuous three-dimensional porous stereoscopic network structure, which is formed after polymer phase separation and ice crystal sublimation during the freeze-drying process. These porous structures enable the hydrogel to absorb exudate and hold large amounts of water, in addition to allowing the hydrogel to provide oxygen and nutrients to cells during wound healing.

Fourier transform infrared spectroscopy (FTIR) is an important method to study the structure and surface functional groups of materials. As shown in **Figure 3**(b), in the infrared spectrum of Curcumin/GQDs, the characteristic peak at 3253 cm^{-1} corresponds to the stretching vibration of O-H and N-H groups, and the absorption peak at 1651 cm^{-1} and 1538 cm^{-1} corresponds to the C=O vibration of carboxylic acid groups and the C=C stretching vibration of aromatic ring skeleton, respectively. The results show that there are abundant oxygen and nitrogen functional groups in GQDs. In addition, the characteristic peaks at 781 cm^{-1} and 455 cm^{-1} may be related to the vibration of C-C, further confirming the structural characteristics of GQDs. In the composite hydrogel Curcumin/GQDs@OHA-CMCS, the slight blue shift of the O-H/N-H vibration peak (3441 cm^{-1}) and the C-H stretching peak (2923 cm^{-1}) indicated the enhancement of the hydrogen bond network. At the same time, the shift of 1623 cm^{-1} peak to 1615 cm^{-1} suggests that coordination between carboxylic acid groups and Curcumin/GQDs may be formed. In addition, the new peaks at 1052 cm^{-1} may correspond to a change in the configuration of C-O bonds, while the low frequency absorption peaks at 706 cm^{-1} and 533 cm^{-1} may be derived from the characteristic vibrations of inorganic structures in the Curcumin/GQDs or from new chemical bonds formed by composite crosslinking. The changes of the above characteristic peaks together verified that Curcumin/GQDs and OHA-CMCS formed a stable composite hydrogel structure through chemical crosslinking and physical interaction.
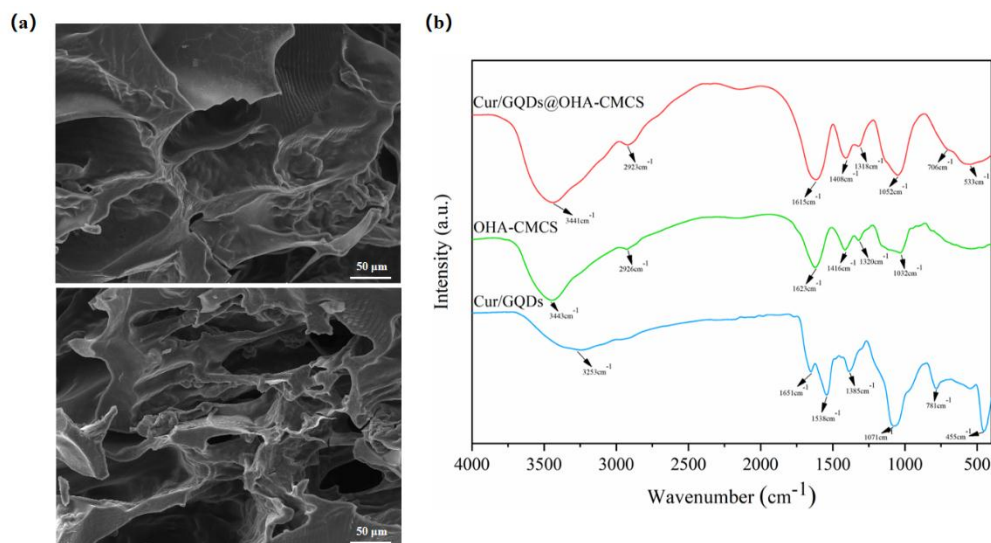
Figure 3 (a)SEM images and (b)IR spectra of CG@OC hydrogels

3.3 Study on rheological properties of hydrogels

Figure 4(a) shows the viscoelastic variation curves of the storage modulus G 'and loss modulus G "of hydrogel with the angular frequency, where the angular frequency varies from 0.1-100 rad/s. It can be seen from the figure that in the whole scanning frequency range, the storage modulus G 'of CG@OC hydrogel sample is greater than its loss modulus G ", which indicates that the elastic deformation of the hydrogel is greater than its viscous deformation, indicating that the hydrogel has a stable cross-linked structure. Time scanning of CG@OC hydrogel was carried out by rheometer, as shown in **Figure 4**(b). The G 'value of CG@OC hydrogel finally stabilized to 1547 Pa, which was slightly higher than that of CCM20@OC hydrogel, indicating that the cross-linking density of the hydrogel network was greater after the addition of Curcumin/GQDs, and therefore its G' value was greater. The greater the G 'value, the better the elasticity of the material.
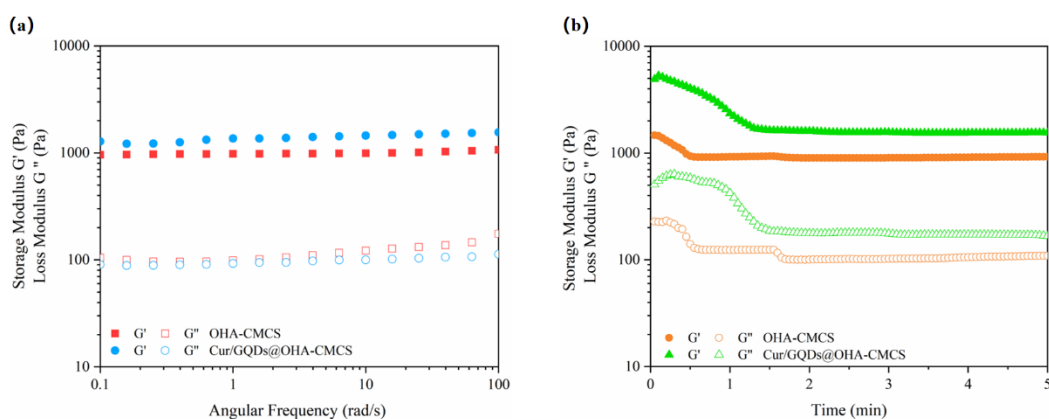

Figure 4 (a)Dynamic frequency sweep measurements and (b)time sweep measurements of OHA-CMCS and CG@OC hydrogels

Rheological recovery tests can study the self-healing properties of hydrogels from a microscopic perspective. As shown in **Figure 5**(a). When the shear strain ranges from 0.1% to 100%, the changes of the storage modulus G "and the loss modulus G" are not obvious, and the storage modulus G "is greater than the loss modulus G", indicating that the elastic deformation of the hydrogel is dominant, and the hydrogel structure is relatively stable at this time. With the increase of strain value, both the energy storage modulus and the loss modulus decrease significantly. As can be seen from the figure, the two curves cross near $\gamma = 214\%$, at which time the energy storage modulus G "" is equal to the loss modulus G". When the strain continues to increase, the loss modulus G "begins to be greater than the energy storage modulus G". This indicated that the polymer molecular chain in the hydrogel sample had changed significantly and the hydrogel cross-linking network had been destroyed. Therefore, $\gamma = 214\%$ can be defined as the strain value corresponding to the gel-sol transition point of CG@OC hydrogel sample. After that, the self-healing ability of CG@OC hydrogel was tested by dynamic rheological

experiment. By determining the sol-gel point, γ = 1% can be taken as a small strain, γ = 300% as a large strain, the hydrogel will be destroyed at a large strain, and will be restored at a small strain. As shown in **Figure 5**(b), in the initial stage, G '> G "indicates that the hydrogel can maintain the stability of its own cross-linking network at this time. Then, when the shear strain increases to 300%, G "< G", the energy storage modulus decreases rapidly from 2451 Pa to 198.17 Pa. At this time, the hydrogel network is destroyed by external forces, showing a viscoelastic state. However, when the large stress of the hydrogel is removed, under the condition of small strain γ = 1%, the energy storage modulus of CG@OC hydrogel can quickly recover the mechanical modulus before the failure, G "> G" again, that is, the hydrogel recovers to the initial stable cross-linked network. This cyclic process validates the hydrogel's self-healing behavior.
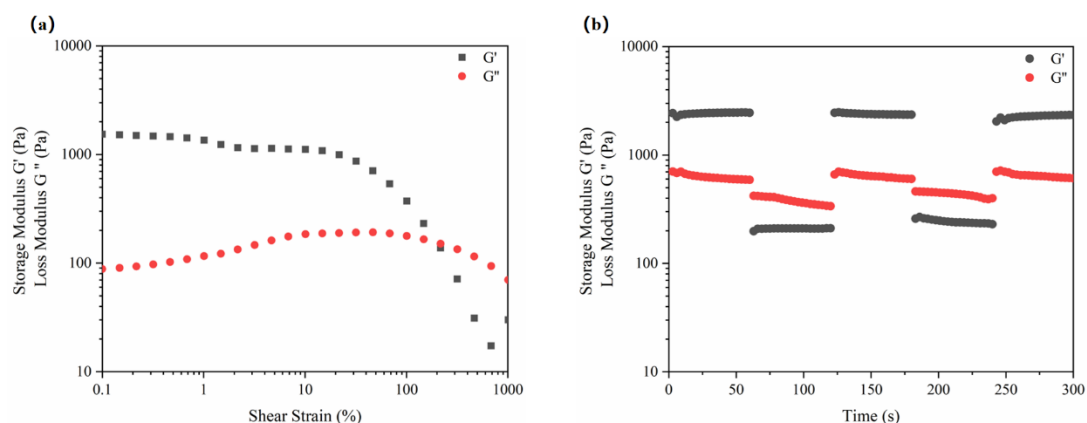

Figure 5 (a)Strain amplitude sweep measurements and (b)Step-strain measurements of CG@OC hydrogels

3.4 Study on hydrogel self-healing behavior

Macro self-healing tests were performed to evaluate the self-healing ability of CG@OC hydrogel. As shown in
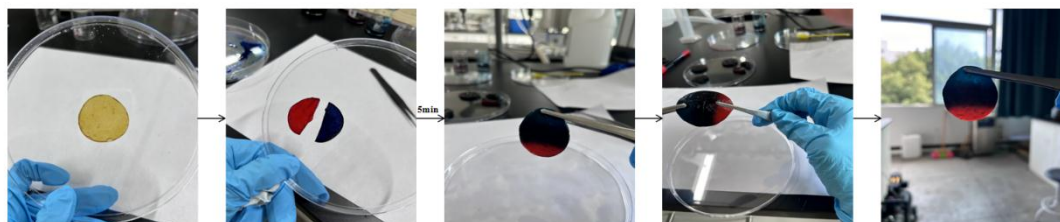

Figure 6, it can be seen that after standing for 5 minutes, the cut part in the middle of the two spliced hydrogels has been connected together, and certain dye penetration occurs on the contact surface of the two hydrogels, indicating that the amino and aldehyde groups on the surface of the two hydrogels have been cross-linked again, and self-healing has been successfully completed. In the stretched state, the hydrogel did not break at the adhesive, indicating that the hydrogel still had certain compressive resistance after self-healing.
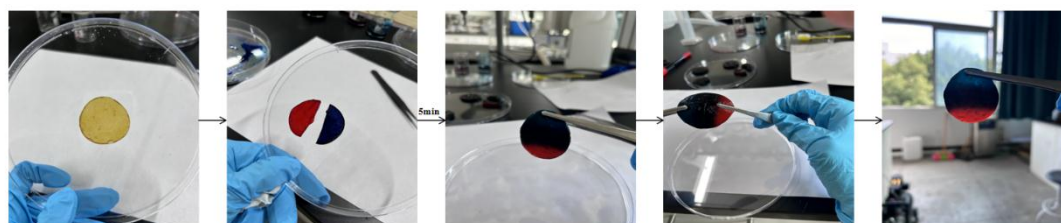

Figure 6 CG@OC self-healing behavior of hydrogels

3.5 Study on drug release performance of hydrogels

As shown in Figure 3-8, curcumin release behavior of Curcumin/GQDs@OHA-CMCS hydrogel showed certain differences at pH 7.4 and 5.5. The experimental results showed that the hydrogel system exhibited slowly

release behavior at both pH conditions, and the acidic environment significantly promoted the late release of curcumin. In a neutral pH 7.4 environment, the cumulative release of curcumin gradually increased with time, but the overall release rate was relatively slow, with a cumulative release rate of about 45.18% within 7 days. In the acidic environment with pH 5.5, the release rate of curcumin increased significantly, and the cumulative release rate reached 51.06% in 7 days. There were significant differences in the release kinetics of the two pH conditions: the release rate of the neutral environment slowed down significantly after the 4th day, while the acidic condition maintained a high release activity. This PH-dependent release behavior may be related to the π-π accumulation of curcumin and GQDs in the structure of the hydrogel network, and the degradation of the hydrogel due to the dissociation of Schiff base bonds triggered by slightly acidic conditions - the protonation effect in the acidic environment weakens the intermolecular force and promotes the dissociation of the drug from the cross-linked network.
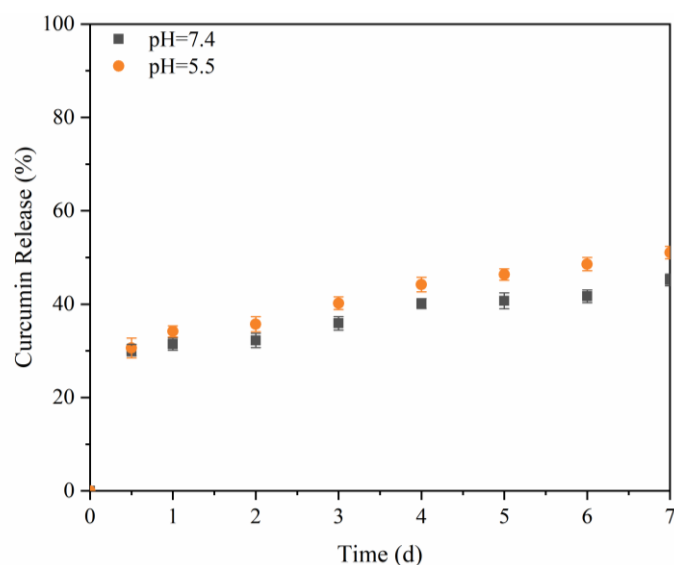

Figure 7 Cumulative release of curcumin from CG@OC hydrogel

3.6 Analysis of hydrogel cytotoxicity test results
The cell compatibility of hydrogel extract was tested by CCK-8 method. The cell survival rate of OHA-CMCS treated with CG@OC hydrogel extract for 48 h was shown in **Figure 8**. Compared with the control group, the survival rate of BEAS-2B cells in hydrogel treatment group was more than 70%.
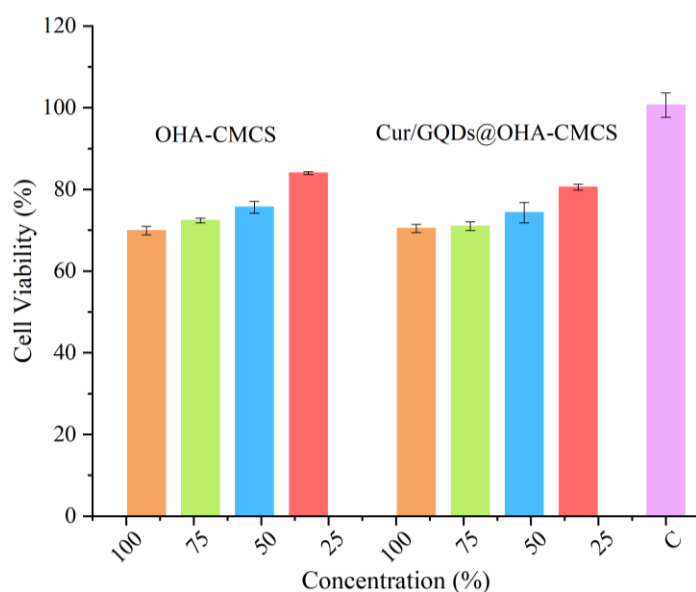

Figure 8 Cytocompatibility results of OHA-CMCS and CG@OC hydrogels

3.7 Analysis of test results of antibacterial properties of hydrogel
Inhibition circle tests of OHA-CMCS and CG@OC hydrogel samples were carried out. As shown in

Figure 9, the bacterial inhibition circle test showed that the hydrogel containing Curcumin/GQDs produced larger bacterial inhibition circle than the hydrogel without Curcumin/GQDs. In addition, OHA-CMCS hydrogels also have certain antibacterial properties, which may be related to the positively charged groups (such as amino groups) of carboxymethyl chitosan, which can bind to the negatively charged groups of bacterial cell membranes, destroy the integrity of the cell membrane, and thus inhibit the growth of bacteria. However, because carboxymethyl chitosan CMCS in OHA-CMCS hydrogels are polymer and form a complex cross-linking network with OHA, the antibacterial properties of CMCS cannot be released, so the antibacterial effect of OHA-CMCS is not obvious in the antibacterial zone experiment.
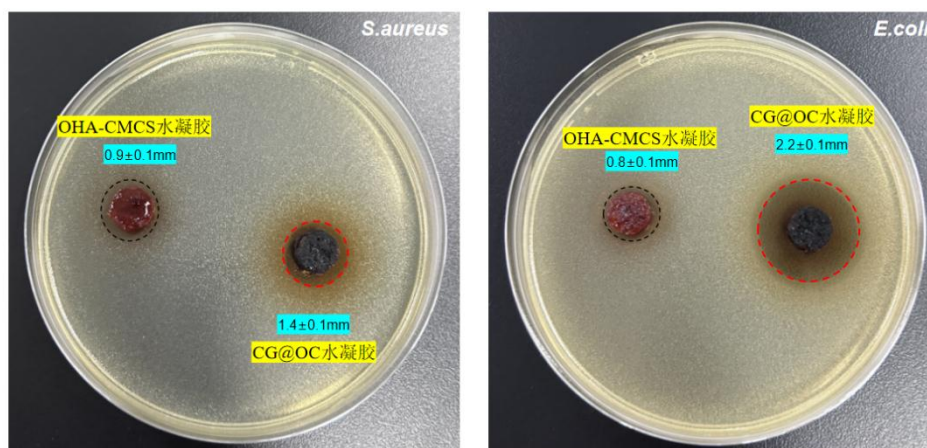

Figure 9 Antibacterial zone effect of CG@OC hydrogels

IV.   Conclusions

In this study, amino-functionalized graphene quantum dots (GQDs) were successfully prepared by a high-temperature hydrothermal method using pyrene nitrate as a precursor. The optimized process conditions were: after oxidation of pyrene monomer by concentrated nitric acid, the reaction was assisted by ammonia-assisted ultrasonic dispersion and reacted at 200 °C for 10 h. Finally, GQDs-NH$_2$ materials were obtained by dialysis purification. The efficient loading of Curcumin Cur on the surface of GQDs was further achieved by π-π stacking and hydrogen bonding to construct the Curcumin/GQDs composite drug-carrying system. Dynamic cross-linking strategy was used to construct OHA-CMCS composite hydrogel matrix. Based on the dynamic Schiff base reaction between the aldehyde group of oxidized hyaluronic acid (OHA) and the amino group of carboxymethyl chitosan (CMCS), a three-dimensional interpenetrating network structure was composited at a volume ratio of 1:2, and the Curcumin/GQDs complex was embedded in synchrony to achieve the functionalization modification. The comprehensive performance evaluation of the Curcumin/GQDs@OHA-CMCS hydrogel indicated that: rheological tests confirmed that it had both the shear-thinning behavior with the Rheological tests confirmed that it has both shear-thinning behavior and rapid self-recovery ability, and macro self-healing experiments showed that the section was healed within 5 min; drug release experiments confirmed that Cur has a pH-responsive release behavior, and the cumulative release reached 51.06% in 7 d under micro-acidic conditions (pH 5.5), and the combination of fluorescent properties of GQDs can achieve real-time monitoring of the drug release process. The CCK-8 experiment confirmed that the cell survival rate was >70%, which demonstrated a certain degree of biosafety; the antimicrobial experiments showed that the hydrogel samples had good antimicrobial properties against Escherichia coli and Staphylococcus aureus. In this work, GQDs were innovatively introduced into the hydrogel system, and the integration of mechanical properties, drug delivery efficiency and fluorescence monitoring function was achieved through the synergistic effect of multi-components, which provided a new idea for the development of new smart hydrogels with both efficient drug loading, intelligent release and real-time monitoring functions.

References

[1] Zeng R, Lin C, Lin Z, et al. Approaches to cutaneous wound healing: basics and future directions[J]. Cell and tissue research, 2018, 374: 217-232.

[2] Xiaobing Fu, Theory and practice of prevention and treatment of chronic difficult-to-heal wounds [J]. People's Health, 2011.

[3] Borena B M, Martens A, Broeckx S Y, et al. Regenerative skin wound healing in mammals: state-of-the-art on growth factor and stem cell based treatments[J]. Cellular Physiology and Biochemistry, 2015, 36(1): 1-23.

[4] Rajakumari K. Skin wound healing: an update on the current knowledge and concepts[J]. Research Journal of Pharmacy and Technology, 2019, 12(3): 1448-1452.

[5] Noor A, Afzal A, Masood R, et al. Dressings for burn wound: a review[J]. Journal of Materials Science, 2022, 57(12): 6536-6572.

[6] Li J, Xue B. Insight into new medical dressings: Classification and characteristics[J]. Chinese Journal of Tissue Engineering Research, 2013, 17(12): 2225.

[7] Li J, Geng L, Wang G, et al. Self-healable gels for use in wearable devices[J]. Chemistry of Materials, 2017, 29(21): 8932-8952.

[8] Nagy P. Kinetics and mechanisms of thiol–disulfide exchange covering direct substitution and thiol oxidation-mediated pathways[J]. Antioxidants & redox signaling, 2013, 18(13): 1623-1641.

[9] Xu J, Liu Y, Hsu S. Hydrogels based on Schiff base linkages for biomedical applications[J]. Molecules, 2019, 24(16): 3005.

[10] Ahmadian Z, Gheybi H, Adeli M. Efficient wound healing by antibacterial property: Advances and trends of hydrogels, hydrogel-metal NP composites and photothermal therapy platforms[J]. Journal of Drug Delivery Science and Technology, 2022, 73: 103458.

[11] Xu Y, Li Y, Chen Q, et al. Injectable and self-healing chitosan hydrogel based on imine bonds: design and therapeutic applications[J]. International journal of molecular sciences, 2018, 19(8): 2198.

[12] Yang L, Wang C, Li L, et al. Bioinspired integration of naturally occurring molecules towards universal and smart antibacterial coatings[J]. Advanced Functional Materials, 2022, 32(4): 2108749.

[13] Chen T, Chen Y, Rehman H U, et al. Ultratough, self-healing, and tissue-adhesive hydrogel for wound dressing[J]. ACS applied materials & interfaces, 2018, 10(39): 33523-33531.

[14] Li W, Cai J, Zhou W, et al. Poly (aspartic acid)-based self-healing hydrogel with precise antibacterial ability for rapid infected-wound repairing[J]. Colloids and Surfaces B: Biointerfaces, 2023, 221: 112982.

[15] Mo C, Xiang L, Chen Y. Advances in Injectable and Self- healing Polysaccharide Hydrogel Based on the Schiff Base Reaction[J]. Macromolecular rapid communications, 2021, 42(10): 2100025.

[16] Wei Z, Yang J H, Liu Z Q, et al. Novel biocompatible polysaccharide- based self- healing hydrogel[J]. Advanced Functional Materials, 2015, 25(9): 1352-1359.

[17] Wang Y, Adokoh C K, Narain R. Recent development and biomedical applications of self-healing hydrogels[J]. Expert Opinion on Drug Delivery, 2018, 15(1): 77-91.

[18] Qu J, Zhao X, Ma P X, et al. pH-responsive self-healing injectable hydrogel based on N-carboxyethyl chitosan for hepatocellular carcinoma therapy[J]. Acta biomaterialia, 2017, 58: 168-180.

[19] Yang L, Zeng Y, Wu H, et al. An antioxidant self-healing hydrogel for 3D cell cultures[J]. Journal of Materials Chemistry B, 2020, 8(7): 1383-1388.

[20] Yang X, Liu G, Peng L, et al. Highly efficient self- healable and dual responsive cellulose- based hydrogels for controlled release and 3D cell culture[J]. Advanced Functional Materials, 2017, 27(40): 1703174.

[21] Verma D, Supe J, Verma S, et al. Removal of Fluoride from Drinking Water by Utilizing Modified Bagasse Sugarcane as Low-Cost Adsorbents for Bilaspur City, Chhattisgarh[J]. Journal of Environmental Informatics Letter, 2024, 11(2): 69-81.

[22] An H, Yang Y, Zhou Z, et al. Pectin-based injectable and biodegradable self-healing hydrogels for enhanced synergistic anticancer therapy[J]. Acta biomaterialia, 2021, 131: 149-161.

[23] Devi VK A, Shyam R, Palaniappan A, et al. Self-healing hydrogels: Preparation, mechanism and advancement in biomedical applications[J]. Polymers, 2021, 13(21): 3782.

[24] Zhou G, Zhang J, Tai J, et al. Comparison of chitosan microsphere versus O-carboxymethyl chitosan microsphere for drug delivery systems[J]. Journal of Bioactive and Compatible Polymers, 2017, 32(5): 469-486.

[25] Han D, Liu X, Wu S. Metal organic framework-based antibacterial agents and their underlying mechanisms[J]. Chemical Society Reviews, 2022, 51(16): 7138-7169.

[26] Kunnumakkara A B, Shabnam B, Girisa S, et al. Inflammation, NF-κB, and chronic diseases: how are they linked?[J]. Critical Reviews™ in Immunology, 2020, 40(1).

[27] Zou Y, Wang P, Zhang A, et al. Covalent organic framework-incorporated nanofibrous membrane as an intelligent platform for wound dressing[J]. ACS applied materials & interfaces, 2022, 14(7): 8680-8692.

[28] Zakerikhoob M, Abbasi S, Yousefi G, et al. Curcumin-incorporated crosslinked sodium alginate-g-poly (N-isopropyl acrylamide) thermo-responsive hydrogel as an in-situ forming injectable dressing for wound healing: In vitro characterization and in vivo evaluation[J]. Carbohydrate Polymers, 2021, 271: 118434.

[29] Tomeh M A, Hadianamrei R, Zhao X. A review of curcumin and its derivatives as anticancer agents[J]. International journal of molecular sciences, 2019, 20(5): 1033.